

**Supplementary Materials**  
**for**  
***Non-destructive mapping of stress and strain in soft thin films through sound waves***

Guo-Yang Li

*Harvard Medical School and Wellman Center for Photomedicine,  
Massachusetts General Hospital, Boston, MA 02114, United States.*

Artur L Gower

*Department of Mechanical Engineering, University of Sheffield, Sheffield, United Kingdom*

Michel Destrade

*School of Mathematical and Statistical Sciences, NUI Galway, Galway, Ireland;  
Key Laboratory of Soft Machines and Smart Devices of Zhejiang Province and  
Department of Engineering Mechanics, Zhejiang University, Hangzhou, PR China*

Seok-Hyun Yun

*Harvard Medical School and Wellman Center for Photomedicine,  
Massachusetts General Hospital, Boston, MA, USA*

### SUPPLEMENTARY NOTE 1: LAMB WAVES IN A STRESSED FILM

Consider a plate with edges parallel to the Cartesian coordinates  $(x_1, x_2, x_3)$ , where  $-h \leq x_3 \leq h$  so that the plate's current thickness is  $2h$ , as illustrated in Supplementary Figure 1(a). Aligned with this axes are the principal stress  $\sigma_1, \sigma_2, \sigma_3$ , and we assume the faces are stress free, so that  $\sigma_3 = 0$ .

The motion of a Lamb wave travelling along  $x_1$  axis with speed  $v$  and wavenumber  $k$  in an elastic incompressible plate is in general governed by the following dispersion equation [1],

$$\left( \frac{\tanh s_1 kh}{\tanh s_2 kh} \right)^{\pm 1} = \frac{s_2(s_1^2 + 1)^2}{s_1(s_2^2 + 1)^2}, \quad (\text{S.1})$$

for symmetric (+1 exponent) and anti-symmetric modes (-1 exponent), and where  $s_1^2, s_2^2$  are the roots of the quadratic

$$\gamma s^4 - (2\beta - \rho v^2)s^2 + \alpha - \rho v^2 = 0. \quad (\text{S.2})$$

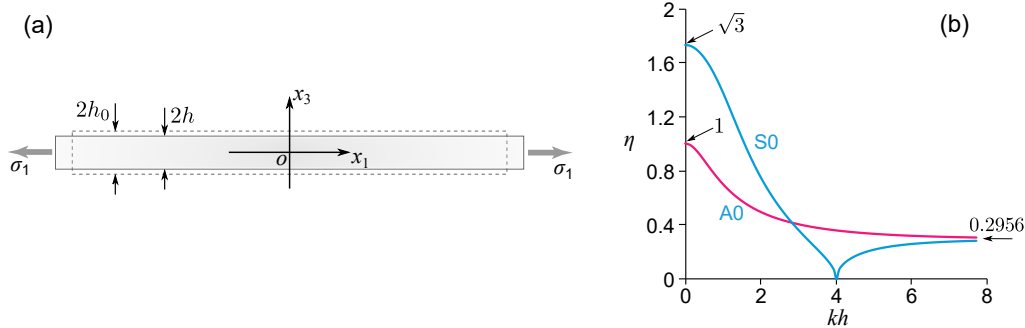
Here  $\alpha, \beta$  and  $\gamma$  are instantaneous elastic moduli, which satisfy

$$\alpha - \gamma = \sigma_1, \quad \alpha/\gamma = \lambda_1^2/\lambda_3^2, \quad (\text{S.3})$$

independent of the materials properties. When the stress are due to an elastic deformation with the pre-stretches  $\lambda_1, \lambda_2, \lambda_3$  along  $(x_1, x_2, x_3)$ , such that  $\lambda_1\lambda_2\lambda_3 = 1$  because of incompressibility, then

$$\alpha = \frac{\sigma_1 - \sigma_3}{\lambda_1^2 - \lambda_3^2} \lambda_1^2, \quad \gamma = \frac{\sigma_1 - \sigma_3}{\lambda_1^2 - \lambda_3^2} \lambda_3^2, \quad 2\beta = \lambda_1^2 \frac{\partial^2 W}{\partial \lambda_1^2} - 2\lambda_1\lambda_3 \frac{\partial^2 W}{\partial \lambda_1 \partial \lambda_3} + \lambda_3^2 \frac{\partial^2 W}{\partial \lambda_3^2} + 2\lambda_1\lambda_3 \frac{\lambda_1 \frac{\partial W}{\partial \lambda_3} - \lambda_3 \frac{\partial W}{\partial \lambda_1}}{\lambda_1^2 - \lambda_3^2}, \quad (\text{S.4})$$

where  $W = W(\lambda_1\lambda_2\lambda_3)$  is the strain energy density, and the identities (S.3) follow immediately. Note that they also hold when the origin of the pre-stress is not known [2, 3].



**Supplementary Figure 1.** (a) Geometry of the stressed film. (b) Master dispersion curves for the fundamental modes, where  $\eta_{A0} = \sqrt{(\alpha - \rho v^2)/\gamma}$ ,  $\eta_{S0} = \sqrt{(\rho v^2 - \alpha)/\gamma}$  when  $kh \leq 3.99$  and  $\eta_{S0} = \sqrt{(\alpha - \rho v^2)/\gamma}$  when  $kh \geq 3.99$ .

Now we consider the strain energy of isotropic incompressible third-order elasticity,

$$W = \mu \text{tr} \mathbf{E}^2 + (A/3) \text{tr} \mathbf{E}^3, \quad (\text{S.5})$$

where  $\mathbf{E}$  is the Green-Lagrange strain tensor,  $\mu$  is the Lamé modulus of linear elasticity ( $\mu = E/3$ , where  $E$  is Young's modulus) and  $A$  is the Landau constant of third-order elasticity (also known as  $n$  in the expansion of Murnaghan). This strain energy is valid up to moderate strain [4]. It can be checked by hand, or with a Computer Algebra System, that when taking a Taylor expansions for small elongations  $\lambda_i - 1$ , we obtain the identity[4]  $2\beta = \alpha + \gamma$ , which substituted into (S.2) leads to

$$s_1^2 = \frac{\alpha - \rho v^2}{\gamma}, \quad s_2^2 = 1, \quad (\text{S.6})$$

and the dispersion equation takes the compact form (Eq. (1) in the main text),

$$4s_1 \left( \frac{\tanh s_1 kh}{\tanh kh} \right)^{\pm 1} = (1 + s_1^2)^2. \quad (\text{S.7})$$

For the fundamental A0 mode, the speed is always subsonic. We define  $\eta_{A0} = \sqrt{(\alpha - \rho v^2)/\gamma}$ , and for each value of  $kh$  we solve

$$4\eta_{A0} \frac{\tanh \eta_{A0} kh}{\tanh kh} = (1 + \eta_{A0}^2)^2, \quad (\text{S.8})$$

numerically for  $\eta_{A0}$ , which leads to the A0 plot on Supplementary Figure 1(b). It starts at  $\eta_{A0} = 1$  as  $kh \rightarrow 0$  and decreases toward 0.2956 (the root of the cubic  $x^3 + x^2 + 3x - 1 = 0$ ) as  $kh \rightarrow \infty$ .

For the S0 modes in the low  $kh$  regime, the wave is supersonic and  $s_1^2 < 0$ . We define  $\eta_{S0} = \sqrt{(\rho v^2 - \alpha)/\gamma}$  and for each value of  $kh$  we solve

$$4\eta_{S0} \frac{\tanh kh}{\tan \eta_{S0} kh} = (1 - \eta_{S0}^2)^2, \quad (\text{S.9})$$

numerically for  $\eta_{S0}$ , which leads to the first branch of the S0 plot on Supplementary Figure 1(b). This equation is valid for  $kh \leq 3.9973$  (the root of the equation  $4 \tanh x = x$ ). Finally for  $kh \geq 3.9973$ , we define  $\eta_{S0}$  as  $\eta_{S0} = \sqrt{(\alpha - \rho v^2)/\gamma}$ , and we solve

$$4\eta_{S0} \frac{\tanh kh}{\tanh \eta_{S0} kh} = (1 + \eta_{S0}^2)^2, \quad (\text{S.10})$$

numerically for  $\eta_{S0}$ , which leads to the second branch of the S0 plot in Supplementary Figure 1(b).

In a material with significant *structural* anisotropy (not only strain-induced anisotropy), potentially due to the presence of aligned collagen or fibers, the propagation and wave speed of the Lamb waves are modified accordingly. In that case the strain energy (S.5) is no longer valid. However, our method could potentially be extended to this scenario, or at least to certain special cases of anisotropy.

## SUPPLEMENTARY NOTE 2: SENSITIVITY ANALYSIS

Here we demonstrate how sensitive our prediction is to the stress  $\sigma_1$  when considering small errors in our measurements. We focus on the sensitivity analysis for the anti-symmetric mode A0, as the results for the S0 mode are analogous.

For the analysis, assume for simplicity that for this mode we measure only two wave speeds  $v_1$  and  $v_2$ , corresponding to two different wavenumbers  $k_1$  and  $k_2$ , respectively. We define  $\eta_1 = \sqrt{(\alpha - \rho v_1^2)/\gamma}$  and  $\eta_2 = \sqrt{(\alpha - \rho v_2^2)/\gamma}$ , which we can solve for  $\alpha$  and  $\gamma$ , and substitute into (S.3) to obtain

$$\sigma_1 = \frac{1}{2}(\rho v_1^2 + \rho v_2^2) + \frac{1}{2}(\rho v_1^2 - \rho v_2^2)F, \quad \text{where} \quad F = \frac{\eta_1^2 + \eta_2^2 - 2}{\eta_1^2 - \eta_2^2}. \quad (\text{S.11})$$

There are several potential sources of errors in using this equation to predict the stress, coming from the error in measuring the wave speeds and from the error in estimating the (non-dimensional) wavenumbers  $k_1 h$  and  $k_2 h$ . We investigate the effect of these errors separately.

First we assume there is an error in measuring the wave speeds, which we call  $\rho \delta v_1^2$  and  $\rho \delta v_2^2$ ; the resulting error in the stress  $\delta \sigma_1$ , according to (S.11) is

$$\delta \sigma_1 = \frac{1}{2}\rho \delta v_1^2(1 + F) + \frac{1}{2}\rho \delta v_2^2(1 - F), \quad \text{so that} \quad \frac{|\delta \sigma_1|}{\rho |\delta v^2|} \leq \frac{1}{2}|1 + F| + \frac{1}{2}|1 - F|. \quad (\text{S.12})$$

Here we assumed that  $\delta v_1$  and  $\delta v_2$  are random and uncorrelated, and used  $|\delta v^2|$  to represent the maximum error in the squared velocities. We define  $c_1 = \frac{1}{2}|1 + F| + \frac{1}{2}|1 - F|$  and plot this quantity in Supplementary Figure 2(c).

Next, we assume the wave speeds have been measured correctly, but that there is an error in estimating the wavenumbers, which leads to

$$\delta \sigma_1 = \frac{1}{2}(\rho v_1^2 - \rho v_2^2) \left[ \frac{\partial F}{\partial \eta_1} \delta \eta_1 + \frac{\partial F}{\partial \eta_2} \delta \eta_2 \right]. \quad (\text{S.13})$$

Then, as we assume the wave speeds were measured accurately, we can use the exact relation  $\rho v_1^2 - \rho v_2^2 = \gamma(\eta_2^2 - \eta_1^2)$  to rewrite this equation in the form

$$\delta \sigma_1 = \gamma \frac{\delta \eta_2^2(1 - \eta_1^2) - \delta \eta_1^2(1 - \eta_2^2)}{\eta_1^2 - \eta_2^2}. \quad (\text{S.14})$$

For third-order elasticity (moderate strains) we have  $\gamma \sim \mu$ , the initial shear modulus, which we use below. Any error committed when calculating  $\eta_1$  and  $\eta_2$  will be a result of an error in evaluating  $k_1 h$  and  $k_2 h$ , as shown by equation (S.8). Hence we can write

$$\delta \eta_1^2 = \frac{\partial \eta_1^2}{\partial(k_1 h)} \delta(k_1 h), \quad \delta \eta_2^2 = \frac{\partial \eta_2^2}{\partial(k_2 h)} \delta(k_2 h). \quad (\text{S.15})$$

Now there are two ways to commit the errors  $\delta(k_1 h)$  and  $\delta(k_2 h)$ . The first is to miscalculate the frequencies  $k_1$  and  $k_2$ , which results in  $\delta(k_1 h) = h \delta k_1$  and  $\delta(k_2 h) = h \delta k_2$ , in which case we can assume the errors are uncorrelated and obtain

$$\frac{|\delta \sigma_1|}{\mu |\delta k| h} \leq \left| \frac{\partial \eta_1^2}{\partial(k_1 h)} \right| \frac{|1 - \eta_1^2|}{|\eta_1^2 - \eta_2^2|} + \left| \frac{\partial \eta_2^2}{\partial(k_2 h)} \right| \frac{|1 - \eta_2^2|}{|\eta_1^2 - \eta_2^2|}. \quad (\text{S.16})$$

Note that  $|\sigma_1| < \mu$  for moderate strains, so that the right hand-side is typically smaller than the relative error of the stress. We call  $c_2$  the right hand side of the above inequality and plot it in Supplementary Figure 2(b).

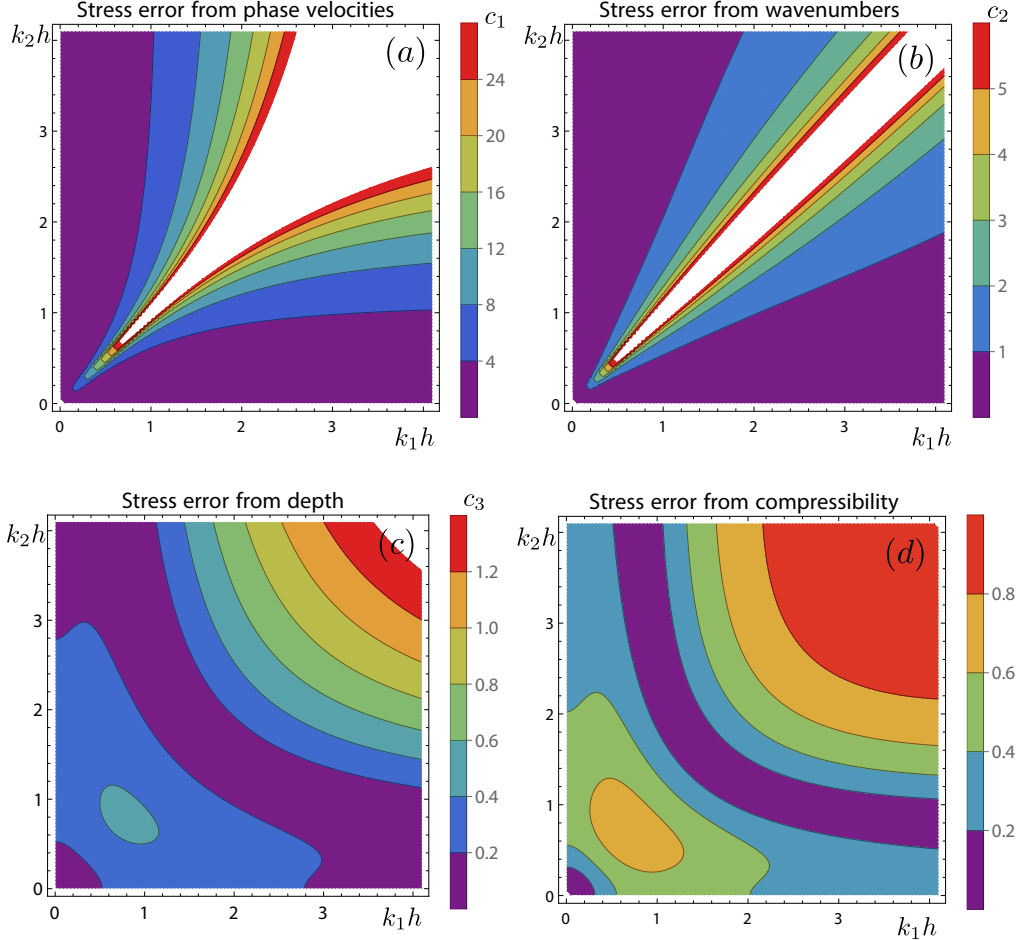
The second way is to miscalculate the film depth  $h$ , which results in  $\delta(hk_1) = k_1 \delta h$  and  $\delta(hk_2) = k_2 \delta h$ , from which we obtain

$$\frac{|\delta \sigma_1|}{\mu |\delta h| h} \leq \frac{1}{|\eta_1^2 - \eta_2^2|} \left| \frac{\partial \eta_1^2}{\partial(k_1 h)} k_1 h (1 - \eta_1^2) - \frac{\partial \eta_2^2}{\partial(k_2 h)} k_2 h (1 - \eta_2^2) \right|. \quad (\text{S.17})$$

We call  $c_3$  the right hand side of this inequality and plot it in Supplementary Figure 2(a).

To summarise, our expected error in predicting the stress, denoted by  $\delta \sigma_1$ , is such that

$$\frac{|\delta \sigma_1|}{\mu} < c_1 \frac{|\rho \delta v^2|}{\mu} + c_2 |\delta k| h + c_3 \frac{|\delta h|}{h}, \quad (\text{S.18})$$



**Supplementary Figure 2.** The graphs show the sensitivity of our prediction of the stress, given by (S.3) due different sources of potential error. In all the figures, it is assumed that the phase speeds  $v_1$  and  $v_2$  of an anti-symmetric Lamb wave are measured at wavenumbers  $k_1$  and  $k_2$ , respectively. For every plot, the white regions have errors larger than the values shown in the accompanying legend. Supplementary 2(a) shows how relative errors in the squared speeds  $v_1^2$  and  $v_2^2$  affect the stress. Supplementary Figure 2(b) shows how errors in estimating  $hk_1$  and  $hk_2$  affect the stress prediction. Supplementary Figure 2(c) shows how errors in estimating the depth  $h$  magnify, or decrease, the errors in predicting the stress. Finally, the values in Supplementary Figure 2(d) times  $\mu/\lambda$  give the error in the stress due to compressibility. For example, if  $\mu/\lambda = 1$ , and  $\mu = 0.02$  GPa, then we would expect an error of 0.016 GPa in the stress when  $k_1 h = k_2 h = 4$ .

where  $\delta h$ ,  $\delta k$ ,  $\delta v$ , are the measurement errors in the sample depth  $h$ , the frequency  $k$ , and the wave speed  $v$ , respectively. The coefficients  $c_1$ ,  $c_2$ ,  $c_3$  depend only on the two frequencies used for the measurement,  $k_1$  and  $k_2$ , and are independent of the material parameters.

For an example, let us consider the measurements made on the rubber membrane, as shown in Figure 1 of the main paper. Its thickness is  $2h \simeq 0.5$  mm. In the case of  $N = 0$  (no weights), at frequency  $f_1 = 2$  kHz, the speed is  $v_1 \simeq 7.5$  m·s<sup>-1</sup>, so that  $k_1 h = 2\pi f_1 h / v_1 = 0.42$ ; at  $f_2 = 16$  kHz the speed is  $v_2 \simeq 13.4$  m·s<sup>-1</sup>, so that  $k_2 h = 1.9$ . For these values of  $k_1 h$  and  $k_2 h$  we find from Supplementary Figure 2 that  $c_2 \sim 0.5$  and  $c_3 \sim 0.3$ . The wavenumber measurement error of our optical coherence tomography (OCT) system is  $\delta k/k \sim 0.1\%$ , see Supplementary Note 5. The thickness measurement error  $\delta h/h \sim 3\%$  is estimated from the error bars of the thickness, see Supplementary Figure 12 (note that it is because the thickness of the sample is not uniform, not because of the spatial resolution of OCT, which is about 0.018 mm.) Therefore, we expect a prediction error  $|\delta\sigma_1|/\mu < 1\%$  (for this calculation, we only included the  $c_2$  and  $c_3$  coefficients, because instead of measuring the speed directly, we calculated it by the formula  $v = 2\pi f/k$ .)

### SUPPLEMENTARY NOTE 3: ALMOST INCOMPRESSIBLE MATERIALS

Our analysis in Section requires that the material be incompressible. Here we show what errors to expect for nearly-incompressible materials.

The equations governing Lamb waves in compressible solids are given by Ogden and Roxburgh [1]. Again, we specialise to third-order elasticity. Then, to take the limit of near-incompressibility, we follow a method used by Shams et al. [4], which in our case leads to taking a series expansion for small  $\mu/\lambda$ , where  $\mu$  and  $\lambda$  are the Lamé constants of linear elasticity. To simplify, and be consistent with third-order elasticity [5], we also consider the strain (or the stress) to be small. The results are

$$\rho v_A^2 = \gamma\eta_A + \alpha + 2(\mu^2/\lambda)F_A(kh), \quad \rho v_S^2 = \alpha - \gamma\eta_S + 2(\mu^2/\lambda)F_S(kh), \quad (\text{S.19})$$

for the anti-symmetric and symmetric modes, respectively. Here, the terms  $F_A(kh)$  and  $F_S(kh)$  depend on  $kh$  only; for example,

$$F_A(kh) = \frac{(S_2 - 2kh)\eta_A^2(1 - \eta_A^2)(1 + \eta_A^2)^2}{S(-4C + khS) - 2((5 + 3C_2)kh - 2S_2)\eta_A^2 + 6S(2C + khS)\eta_A^4 + 4khS^2\eta_A^6 + khS^2\eta_A^8}, \quad (\text{S.20})$$

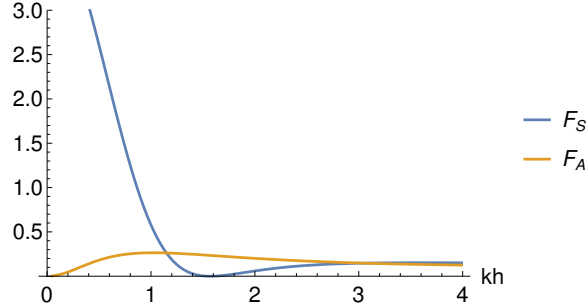
where  $S = \sinh(kh)$ ,  $C = \cosh(kh)$ ,  $S_2 = \sinh(2kh)$ , and  $C_2 = \cosh(2kh)$ . Both  $F_A$  and  $F_S$  are shown in Supplementary Figure 3.

To investigate the error induced by small compressibility, we use (S.12) together with the above to arrive at

$$\frac{|\delta\sigma_1|}{\mu} = \frac{\mu}{\lambda} |F_A(k_1 h)(1 + F) + F_A(k_2 h)(1 - F)|, \quad (\text{S.21})$$

with  $F$  given in (S.11).

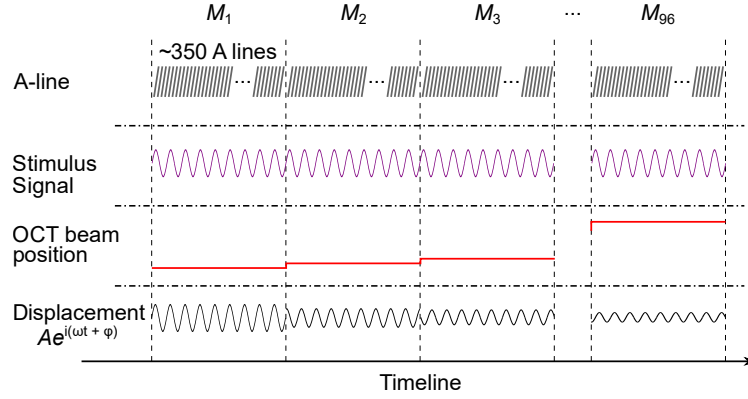
When the material is only slightly compressible,  $\mu/\lambda \ll 1$  and the error is small. However, for more compressible materials,  $\mu/\lambda$  is not small; hence for steel [5],  $\mu/\lambda \simeq 0.8$ . The numerical values of the right hand-side in this equation are shown in Supplementary Figure 2(d).



**Supplementary Figure 3.** Variation of the terms  $F_A$  and  $F_S$  with  $kh$ . When  $F_S$  or  $F_A$  is small, the Lamb wave speed is insensitive to the material compressibility, and conversely when  $F_S$  or  $F_A$  is large.

**SUPPLEMENTARY NOTE 4: M-B SCAN WITH OPTICAL COHERENCE TOMOGRAPHY  
TO MEASURE LAMB WAVE PROPAGATION**

To study and measure Lamb wave propagation, the OCT system works in a M-B scan mode, which is depicted in Supplementary Figure 4. The laser beam scans synchronously with the stimulus signal sent to the PZT. At each lateral location, we acquire  $\sim 350$  A lines (M scan) at a sampling rate of  $\sim 43$  kHz. Then the laser beam moves to the next localisation (B scan). In total 96 lateral locations are measured. The vibration acquired from each M scan is Fourier-transformed to obtain the amplitude  $A$  and phase  $\varphi$ , i.e.,  $u_3(t) = Ae^{i(\omega t + \varphi)}$ . Finally we report the real and imaginary parts of the displacement,  $A \cos(\omega t + \varphi)$  and  $A \sin(\omega t + \varphi)$ , as shown in Figures 5(b) and (d) of the main text.



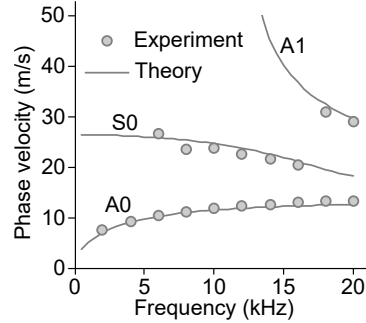
**Supplementary Figure 4.** Schematic of the M-B scan.

**SUPPLEMENTARY NOTE 5: SENSITIVITY IN MEASURING THE WAVENUMBER USING OCT**

The standard deviation in the measurement of the vibration amplitude  $A$  via a single A-line scan, denoted by  $\delta A$ , is given by the optical signal-to-noise ratio (SNR) [6]:  $\delta A = \lambda_0/(4\pi n_0 \sqrt{\text{SNR}})$ , where  $\lambda_0$  is the optical wavelength ( $\sim 1280$  nm) and  $n_0$  is the refractive index ( $\sim 1.4$ ). At the surface of the sample we typically get  $\text{SNR} \approx 40$  dB. This sensitivity is improved by a factor  $1/\sqrt{M}$  upon averaging of  $M$  A-lines. The elastic wave profile is obtained by measuring the displacement at  $N$  locations along the propagation direction and then Fourier-transformed to determine its wavenumber  $k$ . When the beam scan length covers  $\sim 3$  wavelengths, we find that  $\delta k$ , the standard deviation error of the wavenumber, is given by  $\delta k/k \approx \delta A/(A\sqrt{MN})$ . With  $\Delta A = 20$  nm (see Figure 5(d) of the main text),  $M = 350$ , and  $N = 96$ , we obtain  $\delta k/k \approx 0.1\%$ .

**SUPPLEMENTARY NOTE 6: HIGH-ORDER LAMB WAVE MODES  
EXCITED AT HIGH-FREQUENCY RANGE**

When the excitation frequency increases, high-order modes are excited by the probe. Supplementary Figure 5 shows the dispersion relations of the rubber film in the unstressed state. Besides the A0 mode, other wave modes that can be measured from the experiments are also reported. By comparing with the Lamb wave model, it is easy to identify these wave modes as the S0 and A1 modes.

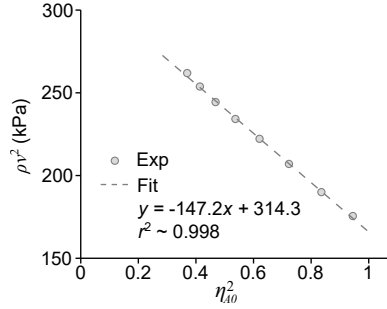


**Supplementary Figure 5.** Dispersion relations of the different Lamb wave modes (A0, S0 and A1) and comparison with theoretical curves. The theoretical curves are computed using the shear modulus obtained from the tensile test.

**SUPPLEMENTARY NOTE 7: MEASURING  $\alpha$  AND  $\gamma$  TO DEDUCE THE STRESS AND STRAIN**

For the fundamental A0 mode, we have  $\rho v^2 = \alpha - \gamma \eta_{A0}^2$ . Thus, we simply need to measure  $v$  at different frequencies: then for each frequency we have a value of  $kh$ , or equivalently, a corresponding value of  $\eta_{A0}^2$ , found by solving (S.8). Then by linear curve fitting we deduce  $\alpha$  (the intercept) and  $\gamma$  (the opposite of the slope) and thus  $\sigma_1$  and  $\lambda_1$  from (S.3).

Supplementary Figure 6 shows the linear regression when the uni-axial stress is due to  $N = 5$  weights, from which we get  $\alpha \simeq 314.3$  kPa and  $\gamma \simeq 147.2$  kPa. According to Eq. (S.3), the stress  $\sigma_1$  is 167.1 kPa and the stretch  $\lambda_1$  is 1.29, which agrees well with the applied stress 162.1 kPa and stretch 1.31.



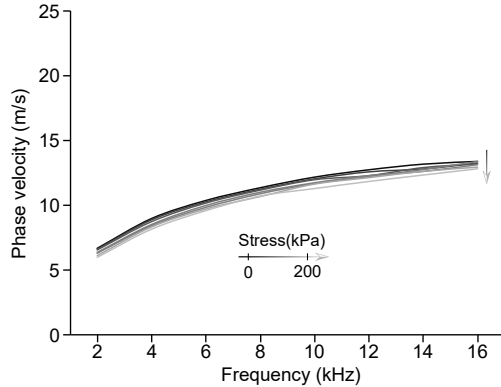
**Supplementary Figure 6.** Representative curve fitting to identify  $\alpha$  and  $\gamma$ . Here  $N = 5$  weights added. The linear fitting of  $\rho v^2$  to  $\eta_{A0}^2$  gives  $\alpha \simeq 314.3$  kPa and  $\gamma \simeq 147.2$  kPa ( $r^2 = 0.998$ ).

**SUPPLEMENTARY NOTE 8: LAMB WAVES TRAVELING  
PERPENDICULAR TO THE UNIAXIAL STRESS**

The analysis for the Lamb wave traveling along  $x_2$  (see Supplementary Figure 7) is the same as that for the wave along  $x_1$ . It yields the elastic moduli  $\alpha'$  and  $\gamma'$ , say, which give

$$\alpha' - \gamma' = \sigma_2, \quad \alpha'/\gamma' = \lambda_2^2/\lambda_3^2. \quad (\text{S.22})$$

For a general biaxial stress state, we solve Eqs. (S.3) and (S.22) to get the stretch ratios  $\lambda_1$  and  $\lambda_2$  (recalling that  $\lambda_1\lambda_2\lambda_3 = 1$ ). In our experiments, the rubber film was uni-axially stretched ( $\lambda_2 = \lambda_3 = \lambda_1^{-1/2}$ ), and we expect  $\alpha' = \gamma'$  and  $\sigma_2 = 0$ .

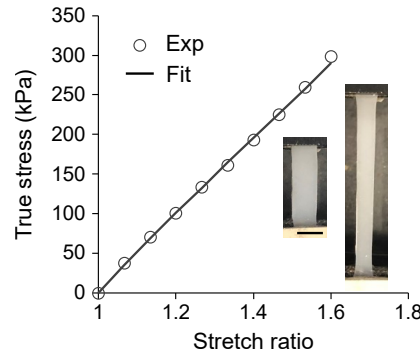


**Supplementary Figure 7.** Dispersion relations of the Lamb waves traveling perpendicular to the uniaxial stress. The phase velocities decrease when the stress increases. Here we find that  $|\sigma_2| < 4$  kPa, which is indeed almost zero compared to  $\sigma_1$ .

**SUPPLEMENTARY NOTE 9: TENSILE TEST OF THE RUBBER FILM**

Supplementary Figure 8 shows the tensile test and the fitting curve. The infinitesimal shear modulus  $\mu \simeq 180$  kPa is obtained by fitting the initial stage (stretch ratio  $< 1.07$ ) of the stretch-stress curve. To fit the whole curve we use the Mooney-Rivlin model  $W = C_{10}(\lambda_1^2 + \lambda_2^2 + \lambda_3^2 - 3) + C_{01}(\lambda_1^2\lambda_2^2 + \lambda_2^2\lambda_3^2 + \lambda_3^2\lambda_1^2 - 3)$ , with  $C_{10} \simeq 51$  kPa and  $C_{01} \simeq 39$  kPa. Then we recall that the Mooney-Rivlin model is equivalent, at the same level of approximation, to the general model of third-order elasticity (S.5), with the connections [7]  $\mu = 2(C_{10} + C_{01})$  and  $A = -8(C_{10} + 2C_{01})$ , or here,  $\mu = 180$  kPa,  $A = -1,302$  kPa.

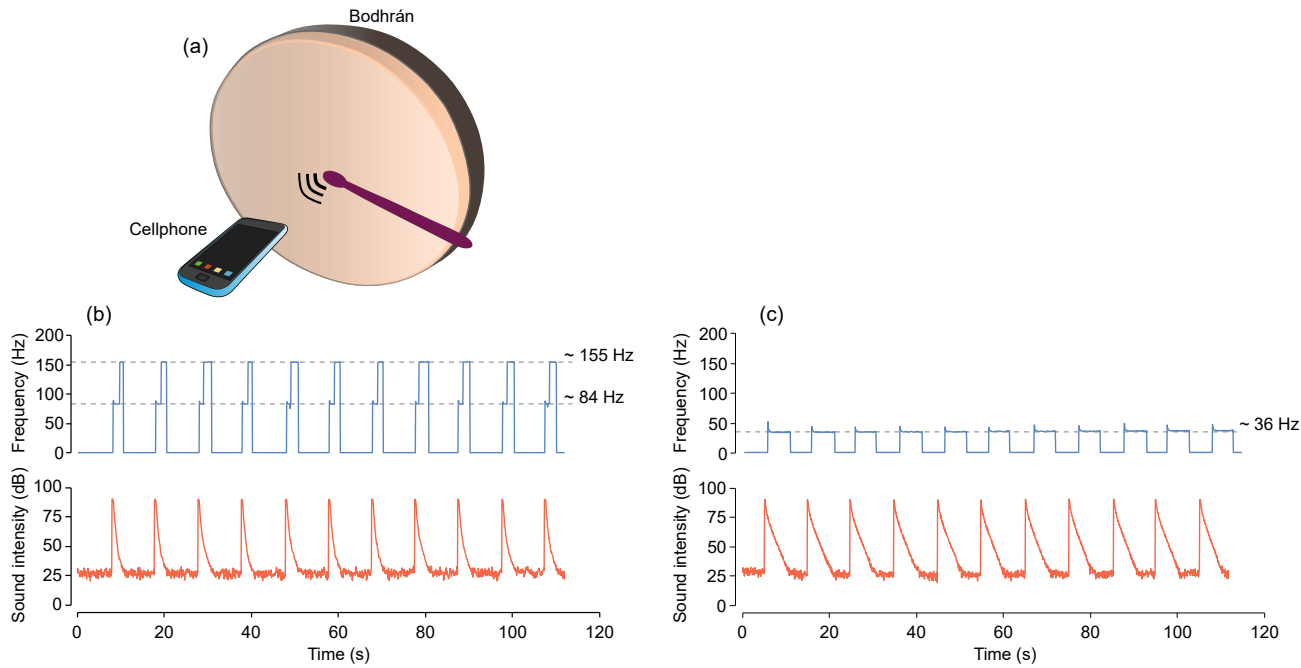
These material parameters are used in the main text to produce theoretical dispersion curves and confirm the match with the experimental data, although ultimately they are not needed for our stress measurement method through OCT imaging.



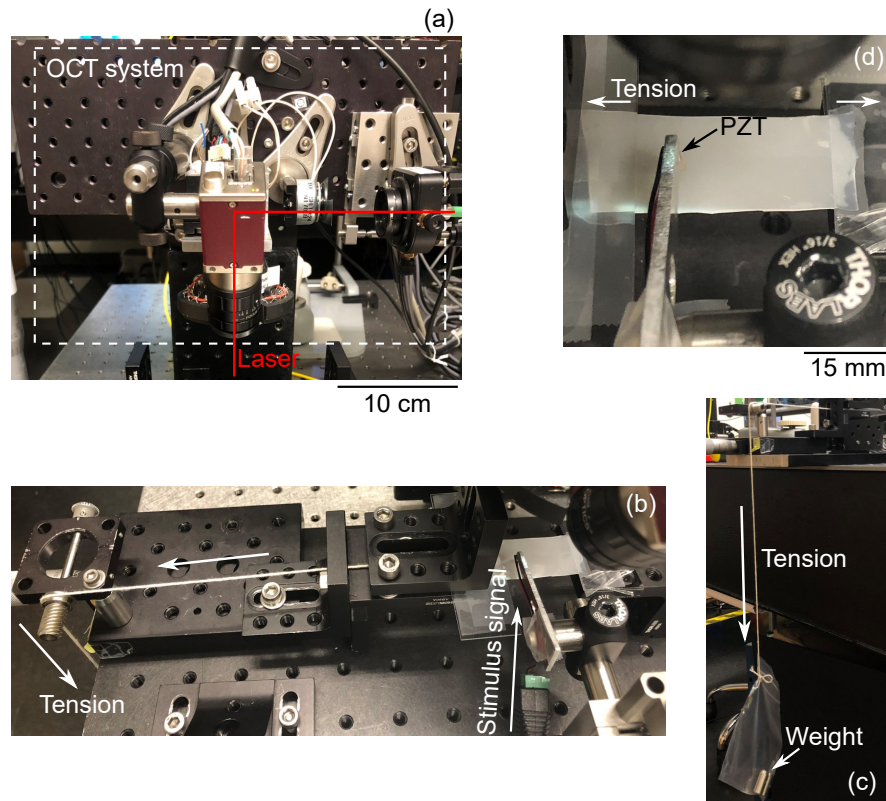
**Supplementary Figure 8.** Tensile test of the rubber film. Inset, photos of the undeformed and deformed sample. Scale bar, 5 mm.

### SUPPLEMENTARY NOTE 10: CHARACTERISATION OF THE BODHRÁN

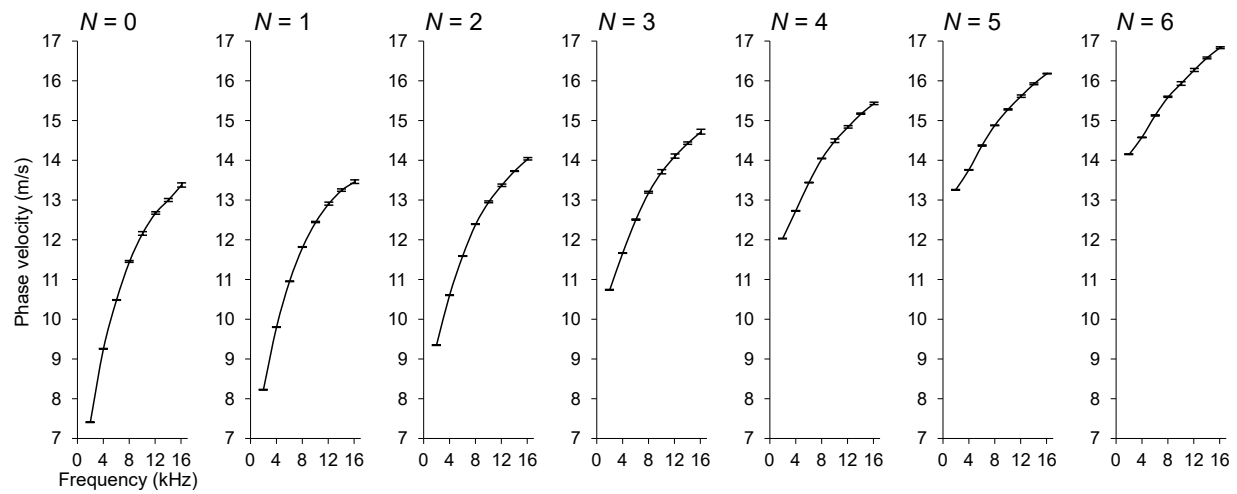
To show that the tension can be reduced by wetting the inner side of the *bodhrán* skin, and so that the vibration frequencies change, we used the experimental setup depicted in Supplementary Figure 9(a) to characterize the fundamental vibration frequencies of the dry and wet *bodhrán*. The *bodhrán* was beaten at its center every 10 seconds and then the sound was measured with a cellphone using the Google Science Journal App. The cellphone was placed about 10 cm away from the skin. As shown in Supplementary Figure 9(b), the fundamental vibration frequency was  $\sim 84$  Hz in the dry state. However, wetting the skin, as shown in Supplementary Figure 9(c), decreases the vibration frequency to  $\sim 36$  Hz.



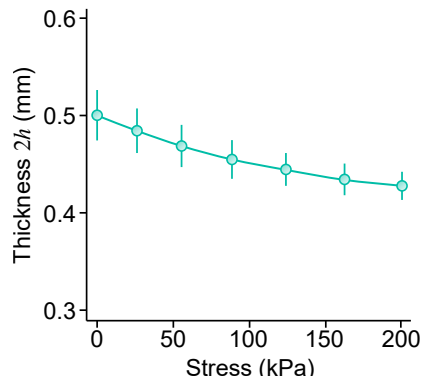
**Supplementary Figure 9.** Vibration frequency of the *bodhrán*. (a) Schematic of the experiment. The *bodhrán* is beaten every 10 seconds and then the sound intensity and frequency are measured by a cellphone. (b) Dry state. The fundamental and second harmonic frequencies can be measured:  $\sim 84$  Hz and  $\sim 155$  Hz. (c) Wet state. The fundamental frequency drops to  $\sim 36$  Hz.



**Supplementary Figure 10.** Photos of the experimental setup. (a) Scanning laser of the OCT system. (b) and (c) show how stress is applied to the film by a simple pulley/weight apparatus. (d) A zoomed-in view of (b) showing the sample and the PZT that is used to drive the vibration of the probe.



**Supplementary Figure 11.** Standard deviations of the experimental data shown in Figure 1(f) of the main text. Here,  $N$  indicates the number of the weights.



**Supplementary Figure 12.** Variation of the rubber sheet thickness (as tracked by OCT) with the stress, from  $N = 0$  (stress-free) to  $N = 6$  weights of 20 g each. As expected, the thickness decreases as we increase the stress, due to the Poisson effect. Error bars indicate standard deviations over five measurements performed at different locations of the sample.

**SUPPLEMENTARY REFERENCES**

- 
- [1] Ogden, R. W. & Roxburgh, D. The effect of pre-stress on the vibration and stability of elastic plates. *International Journal of Engineering Science* **31**, 1611–1639 (1993).
  - [2] Shams, M., Destrade, M. & Ogden, R. W. Initial stresses in elastic solids: Constitutive laws and acoustoelasticity. *Wave Motion* **48**, 552–567 (2011).
  - [3] Gower, A. L., Shearer, T. & Ciarletta, P. A new restriction for initially stressed elastic solids. *Quarterly Journal of Mechanics and Applied Mathematics* **70**, 455–478 (2017).
  - [4] Destrade, M., Gilchrist, M. D. & Saccomandi, G. Third-and fourth-order constants of incompressible soft solids and the acousto-elastic effect. *Journal of the Acoustical Society of America* **127**, 2759–2763 (2010).
  - [5] Li, G.-Y., Gower, A. L. & Destrade, M. An ultrasonic method to measure stress without calibration: The angled shear wave method. *Journal of the Acoustical Society of America* **148**, 3963–3970 (2020).
  - [6] Ramier, A., Cheng, J. T., Ravicz, M. E., Rosowski, J. J. & Yun, S.-H. Mapping the phase and amplitude of ossicular chain motion using sound-synchronous optical coherence vibrography. *Biomedical Optics Express* **9**, 5489–5502 (2018).
  - [7] Destrade, M., Gilchrist, M. D., Murphy, J.G. Onset of nonlinearity in the elastic bending of blocks. *Journal of Applied Mechanics* **77**, 061015 (2010).